Heliyon 8 (2022) e10309

Contents lists available at ScienceDirect

Heliyon

journal homepage: www.cell.com/heliyon

Research article

A GIS and remote sensing approach for measuring summer-winter variation of land use and land cover indices and surface temperature in Dhaka district, Bangladesh

Mizbah Ahmed Sresto, Sharmin Siddika, Md. Abdul Fattah *, Syed Riad Morshed, Md. Manjur Morshed

Department of Urban and Regional Planning, Khulna University of Engineering and Technology, Khulna, 9203, Bangladesh

ARTICLE INFO

Keywords:
Land use change
Land surface temperature
Season variation
Remote sensing
Urban ecology

ABSTRACT

Rapid urbanization has induced land use and land cover change (LULC) that increases land surface temperature (LST). Analyzing seasonal variations of LULC and LST is a precondition for mitigating heat island effects and promoting a sustainable living environment. The objective of this study is to explore the association between the seasonal LST dynamics and LULC indices for the Dhaka district of Bangladesh. The LULC indices are comprised of the Normalized Difference Vegetation Index (NDVI), Normalized Difference Built-up Index (NDBI), Normalized Difference Bareness Index (NDBAI), and Modified Normalized Difference Water Index (MNDWI). The results show that the LULC effect on LST in Dhaka is significant, with an increase in summer season LST from 34.58 °C to 37.66 °C and in winter season LST from 24.710C to 26.24 °C. Predictably, the highest and lowest LST values were observed in the built-up and vegetation-covered areas, respectively. Secondly, the correlation values indicate a significant inverse correlation ($R^2 > 0.50$) between NDVI and LST, as well as MNDWI and LST. On the contrary, positive correlations were observed between NDBI and LST, and between NDBAI and LST for both the summer and winter seasons. Finally, subsequent vegetation decline (-69.34%) and increasing built-up area (+11.30%) between 2000 and 2020 in Dhaka district were found to be the most significant factors for the increasing trend and spatial heterogeneity of LST in Dhaka. The methodological approach of this study offers a low-cost efficient technique for monitoring LST hotspots, which can guide land use planners and urban managers for spatial intervention to ensure a livable environment.

1. Introduction

Climate and land use are interrelated with each other. Changes in land use and land cover (LULC) can affect and can be affected by climate. At various temporal and spatial dimensions, these changes interact; however, improper LULC change is the primary reason for climate change (Thakur et al., 2019; Mondal et al., 2021a, b; Fattah and Morshed 2022). The problem is most prominent in urban areas, especially in emerging cities. With the population growth and development of cities, city planning and management must confront an increasing number of challenges, including urban climatic effects. An increase in land surface temperature (LST) due to manmade and natural reasons is currently one of the most critical urban climate effects. Furthermore, the effects of rising LST have been linked to a variety of negative urban effects, including reduced comfort, deterioration of air and water quality, increased mortality rates, and indirect economic losses (Steeneveld et al., 2018; Kafy et al., 2022). The study of LULC and its impacts has become a research hotspot in urban planning as well as urban meteorology, ecology, and geography. Moreover, for adopting sustainable adaptation measures, more improved information and knowledge is required about the magnitude and extent of LST dynamics as well as seasonal LST dynamics caused by rapid urban expansion, especially in developing megacities like Dhaka.

LULC changes can occur as a result of both human and climate-related factors. Demand for additional settlements, for example, frequently results in the irreversible loss of working and natural land cover, which can lead to localized changes in weather patterns, precipitation, and temperature (Morshed et al., 2021; Mondal et al., 2021a, b, 2022; Thakur et al., 2020a, 2020b; Gazi and Mondal 2018). These changes have the ability to influence the Earth's climate by modifying local, regional, and

* Corresponding author.
E-mail address: mafattah.kuet@gmail.com (Md.A. Fattah).

https://doi.org/10.1016/j.heliyon.2022.e10309
Received 21 February 2022; Received in revised form 5 June 2022; Accepted 11 August 2022

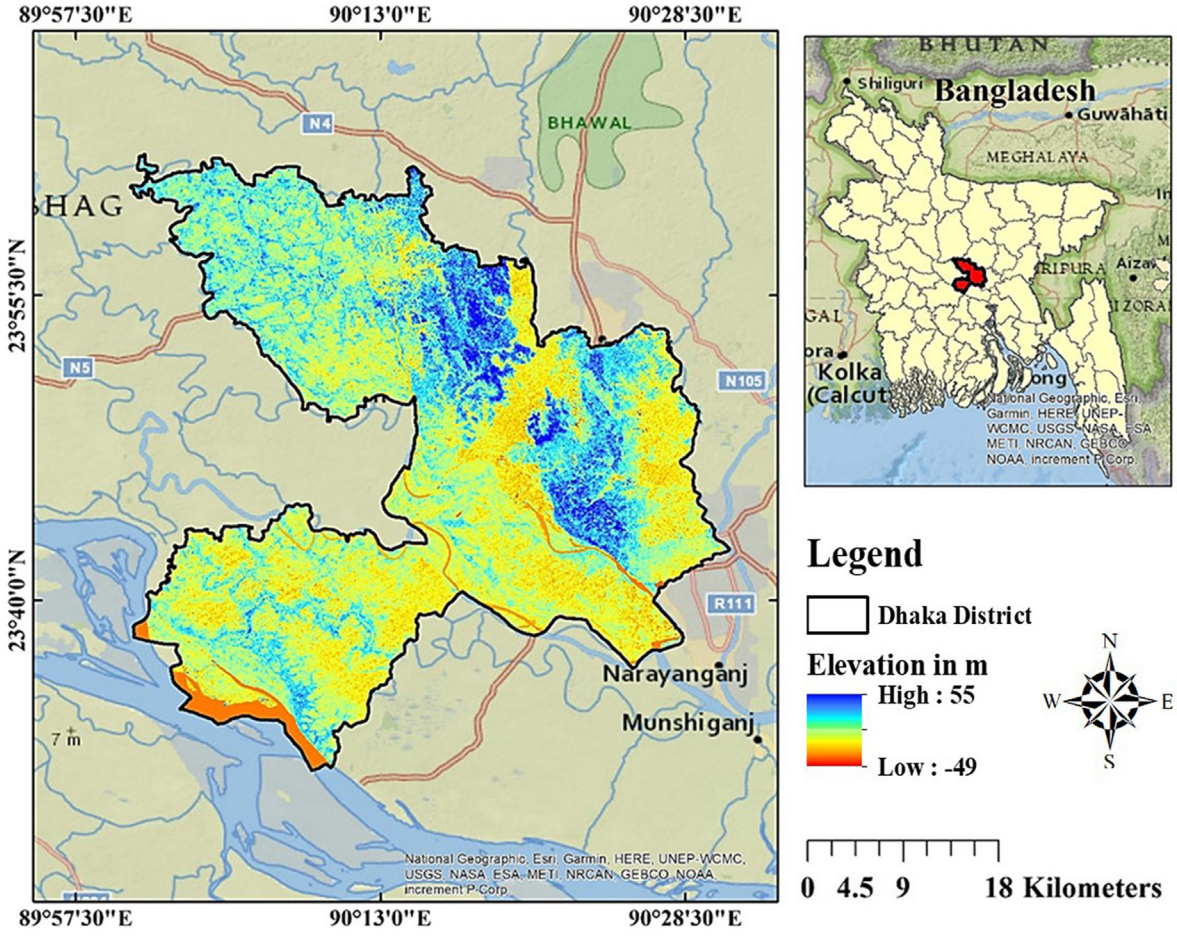

Figure 1. District map of Dhaka, Bangladesh.

global circulation patterns, changing the reflectivity of the Earth's surface, and increasing the CO2 in the atmosphere when they are accumulated over huge areas (Fattah et al., 2021a). An increase in built-up areas decreases the eco-friendly land cover types such as forest land, vegetation, and waterbodies, which affect the ecosystem and therefore carbon storage (Kumar et al., 2021; Thakur et al., 2019; Mondal et al., 2018, 2021a, b). The transformation of land cover to built-up areas in the urban areas accounted for the increased carbon emissions and the decline in carbon sequestration. This phenomenon is leading to global warming as well as increases in LST (Fattah et al., 2021b; Thakur et al., 2019; Mondal et al., 2021a, b). Though different regions across the world have been facing the adverse impacts of LULC change as well as LST growth, the impacts are more acute in the developed cities. The association between LULC and LST is attracting increasing attention from the scientific community, health authorities, urban planners, and environmental engineers because of its substantial impacts on human health, raised energy demand for colling and altered vegetation phenology (Li et al., 2017; Lowe, 2016; Lemonsu et al., 2013).

$$User\ Accuracy = \frac{cor\ rectly\ classified\ points\ in\ each\ category\ (diagonal)}{Total\ reference\ points\ in\ each\ category\ (row\ total)} * 100 \quad (3)$$

$$Producer\ Accuracy = \frac{cor\ rectly\ classified\ points\ in\ each\ category\ (diagonal)}{\text{Total reference points in each category (column total)}} * 100 \quad (4)$$

Table 1. Details of the utilized Landsat images (https://earthexplorer.usgs.gov/).

Years	Acquisition date	Satellite	Sensor	Path/ Row	Cloud coverage
2000 Summer	2000-04-10	Landsat 5	TM	137/44	<10%
	2000-04-10	Landsat 5	TM	137/43	<10%
2010 Summer	2010-04-07	Landsat 5	TM	137/44	<10%
	2010-04-07	Landsat 5	TM	137/43	<10%
2020 Summer	2020-04-18	Landsat 8	OLI	137/44	<10%
2000 Winter	2000-12-20	Landsat 5	TM	137/44	<10%
	2000-12-20	Landsat 5	TM	137/43	<10%
2010 Winter	2010-01-02	Landsat 5	TM	137/44	<10%
	2010-01-02	Landsat 5	TM	137/43	<10%
2020 Winter	2020-12-27	Landsat 8	OLI	137/44	<10%

Table 2. LULC classes and corresponding land use types.

Classes	Description
Waterbody	Wetlands, gully, marshy land, low-lying lands and gully.
Built-up	Residential, industrial, commercial areas, settlements, roads, mixed urban areas, impervious covers.
Bare land	Open space, landfill sites, brickfields, barren soil, construction sites, abandoned land, uncultivated land.
Agriculture land	Crop fields, fruits and other cultivated lands, fallow lands.
Vegetation	Forest and trees, vegetative lands, mixed forest land, gardens.

Table 3. The NDVI value ranges indicates different LULC types, used for LST distribution (Akbar et al., 2019).

Classes	NDVI value ranges
Waterbody	−0.28 to -0.015
Built-up	-0.014 to +0.13
Bare land	+0.14 to +0.18
Agriculture land	+0.19 to +0.27
Vegetation	+0.27 to +0.36
Dense vegetation	+0.36 to +0.74

$$Overall\ Accuracy = \frac{\text{Total cor rectly classified points (diagonal)}}{\text{Total reference points}} * 100 \quad (5)$$

$$Kappa\ Cofficient = \frac{\text{Total Sample} * \text{Total Cor rect Sample} - \sum(\text{column.total} * \text{row total})}{(\text{Total Sample})^2 - \sum(\text{column.total} * \text{row total})} * 100 \quad (6)$$

LST is a very important parameter for both local and global energy and water balances at the surface. Remote sensing sensors made it easier to study LULC and LST effects more preciously. Currently, many advanced and effective remote sensing technologies are used to estimate LST. The impact of LULC on LST has been widely studied in many prior studies, including Li et al. (2017); Steeneveld et al. (2018); Zhang et al. (2016); Al-Hameedi et al. (2021). Several researches also focused on the major cities of Bangladesh like Dhaka (Faisal et al., 2021); Chittagong (Gazi et al., 2021), Khulna (Fattah et al., 2021a, b), Sylhet (Kafy et al., 2022), Cumilla (Kafy et al., 2021). Although these studies focused on the LULC change effects on LST variations, there is a lack of research that comprehensively compares the seasonal effects. All these studies quantified the LST for only the summer season. In addition, most of the studies used only two common land use indices (NDVI—"Normalized Difference Vegetation Index' and NDBI– 'Normalized Difference Built-up Index') and comprehended the impacts of vegetation cover loss and built-up cover increase on LST change. As a result, water bodies and bare land are frequently overlooked. A limited number of studies explored the influence of all LULC types on LST dynamics. The distribution of LST varies seasonally and responds differently to different LULC classes (Huang and Cadenasso, 2016).

Various land use indices (applied to the Landsat images to characterize different land cover classes) are used to characterize the specific land cover types. For example, NDVI is used to evaluate vegetation, NDBI for built-up cover, MNDWI- 'Modified Normalized Difference Water Index' for soil moisture, and NDBaI- 'Normalized Difference Bareness Index' for soil bareness related issues (Imran et al., 2021). However, in present studies, the use of all these land use indices is rarely explored comprehensively from the combined perspective of seasonal variations. Historical LULC and LST change identification, seasonality analysis, and determining the responses of LST to different land use indices have important application value and scientific research significance. To fill the previous study gap, the present study is designed to analyze the

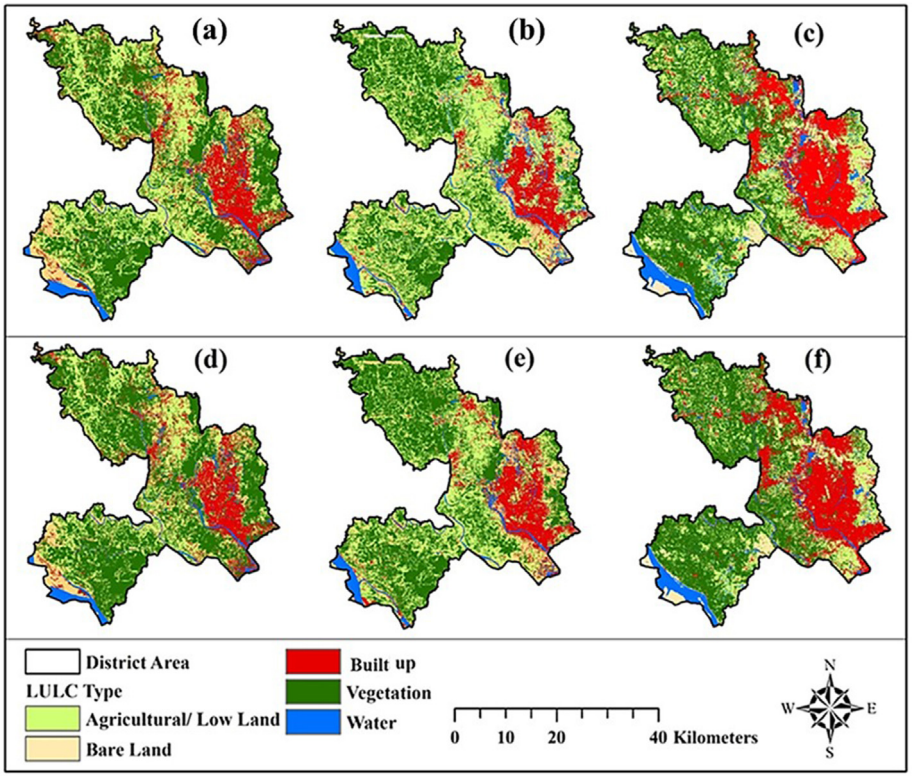

Figure 2. Deprived LULC patterns of Dhaka during winter season of (a) 2000 (b) 2010 (c) 2020 and summer season of (d) 2000 (e) 2010 (f) 2020.

Table 4. Classified LULC statistics of Dhaka district Summer (S) and Winter (W) (area in %).

	2000		2010		2020		Change during 2000 – 2020 (km^2)	
	W	S	W	S	W	S	W	S
AL	23.37	24.19	20.95	21.31	17.01	17.6	-93.45	-96.80
BL	8.65	7.77	8.81	8.34	9.38	8.54	10.64	11.30
BU	14.55	14.48	18.03	17.87	23.19	23.08	126.97	126.32
VG	48.86	49.14	47.82	48.23	44.10	44.83	-69.94	-63.20
WB	4.57	4.43	4.39	4.25	6.32	5.96	25.78	22.38
Total	100	100	100	100	100	100		

VG = Vegetation, AL = Agricultural Land, BU = Built Up, WB = Water Body, BL = Bare Land.

historical LULC and LST trends, seasonal (summer-winter) and spatial distribution of LULC, LST, NDVI, NDBAI, MNDWI, and NDBI from 2000 to 2020 over Dhaka City. Furthermore, the distribution and responses of seasonal LST change to all the land use indices were statistically analyzed. The outcomes of the present study can provide a scientific reference and guidance to urban planners and policy makers to adopt effective mitigation measures in urban development plans.

2. Methods and materials

2.1. Study area

Dhaka district is located between north latitudes 23°53′ and 24°06′ and the east longitudes between 90°01′ and 90°37'. Dhaka district includes Dhamrai, Savar, Dhaka city, Keraniganj, Dohar, and Nawabganj (Imran et al., 2021). The district shares borders with Tangail and Gazipur in the north, Munshiganj in the south, Rajbari and Manikganj districts on the west, and Naraynganj district on the east (Figure 1) (Moniruzzaman et al., 2021). The elevation of Dhaka district ranges from -49 (low) to 55 (high) (according to SRTM 30 m resolution dem) (USGS 200). The climate of Bangladesh can be divided into four distinct seasons: summer (March–May), monsoon (June September), post-monsoon (October–November) and winter (December–February). For being situated in a tropical region, the study area is mostly dry in winter and hot and humid in summer (Begum et al., 2021; BBS 2017).

Dhaka's population is growing at a rate of about 4% per year, which is one of the fastest rates in Asian cities (Swapan et al., 2017). Over the last 50 years (1978–2018), the built-up area of Dhaka city and surrounding areas has increased from 1.7% to 23.8%. Dhaka is the most densely populated city in Bangladesh with 68,561 people per km^2 (Moniruzzaman et al., 2021).

There has been a lot of migration to the Dhaka region and the city's boundaries have been expanded, which has led to a rise in the city's population. In the 1980s, the city added more than a million people to its population (McGee, 2006). This led to rapid urban expansion towards upazilas (tertiary urban centers) around DMA, such as Dhamrai, Savar, Keraniganj, Dohar, and Nawabganj, which are under Dhaka district (Figure 1). To attract foreign investments and provide urban service facilities for people, various types of infrastructure, such as roads and highways, industry, commercial buildings, factories, and so on, were developed in these areas for economic development (Arefin et al., 2019). Though such initiatives will provide communities with economic possibilities and socio-economic benefits, they will result in urban expansions, LULC modifications, and accelerate urban heat islands (UHI) effects in the study area. In this regard, this study considered Dhaka district as the study area to assess the seasonal LST distributions and the influences of different land use factors.

2.2. Data collection

There are four seasons in Bangladesh, summer, pre monsoon, post monsoon and winter (Begum et al., 2021). To assess the seasonal diversity between summer and winter ten Landsat images were collected for analyzing the spatiotemporal changes. To identify the spatial and thermal variations in the summer and winter seasons, different Landsat images were collected as given in Table 1. For both Landsat 8 and 5, Landsat collection 1 level-1 images were assembled for this study. Geographical Information System (GIS) based remote sensing software ArcGIS 10.5 version was utilized to process and analyze the acquired data. Landsat imagery helped to extract the LST, LULC types, and land use indices from Landsat imagery. The shape files of the Dhaka District were collected from Rajdhani Unnayan Kartripakkha (RAJUK) (RAJUK, 2020). RAJUK is responsible for coordinating any development project in Dhaka, Bangladesh.

2.3. Radiometric correction of landsat images

First of all, the mosaic band tool was performed for attaching 2 different landsat-5 images in order to cover the whole study area. On the other hand, one Landsat 8 image covered the whole study area. So, no preprocessing techniques were performed on the Landsat 8 image. All required bands were composited (bands 1 to 5 for the Landsat 5 image).

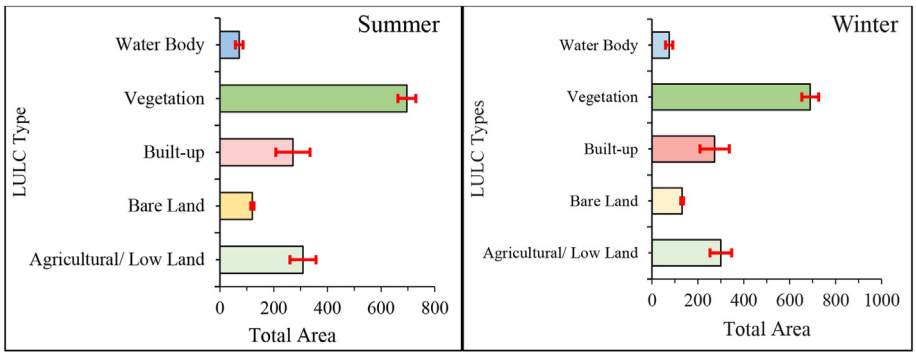

Figure 3. LULC variation ranges (standard deviations) for summer and winter.

Table 5. LULC transition matrix in Dhaka during 2000–2020.

LULC Transition	Transformed area (Summer)		Transformed area (winter)	
	km^2	%	km^2	%
Agriculture - Agricultural	56.05	3.82	58.50	3.98
Bare Land - Agricultural	12.50	0.85	14.62	1.00
Built-up - Agricultural	15.22	1.04	13.86	0.94
Vegetation - Agricultural	195.46	13.31	214.40	14.59
Waterbody - Agricultural	3.71	0.25	3.35	0.23
Agriculture - Bare Land	36.12	2.46	37.76	2.57
Bare Land - Bare Land	18.09	1.23	20.13	1.37
Built-up - Bare Land	9.63	0.66	9.33	0.64
Vegetation - Bare Land	95.90	6.53	108.86	7.41
Waterbody - Bare Land	19.61	1.33	16.51	1.12
Agriculture - Built-up	93.66	6.38	96.37	6.56
Bare land - Built-up	49.63	3.38	50.56	3.44
Built-up - Built-up	159.19	10.84	160.70	10.94
Vegetation - Built-up	103.21	7.03	108.20	7.37
Waterbody - Built-up	15.14	1.03	13.99	0.95
Agriculture - Vegetation	27.82	1.89	22.50	1.53
Bare Land - Vegetation	49.88	3.40	48.29	3.29
Built-up - Vegetation	39.84	2.71	36.57	2.49
Vegetation - Vegetation	370.03	25.19	332.40	22.63
Waterbody - Vegetation	4.67	0.32	2.24	0.15
Agriculture - Waterbody	5.02	0.34	9.67	0.66
Bare Land - Waterbody	20.90	1.42	19.46	1.32
Built-up - Waterbody	3.74	0.25	4.13	0.28
Vegetation - Waterbody	36.80	2.51	38.51	2.62
Waterbody - Waterbody	27.18	1.85	28.10	1.91
Total	1469.00	100	1469.00	100

Geometric, atmospheric and radiometric pre-processing techniques have been used by different researches like Adeyeri et al. (2017) and Nautiyal et al. (2021). The geometric adjustment was performed with the help of proper spatial referencing. FLAASH atmospheric correction was used to reduce noise caused by the atmospheric effect (Abir and Saha, 2021; Akram et al., 2018; Mondal et al., 2016).

To convert DN (a numerical value of each pixel, called a digital number) values into radiance while taking into account the gain and bias of different bands (Eqs. (1) and (2)). We corrected for radiometric errors and translated digital DN data to reflectance levels (Zhang et al., 2016; Dhar et al., 2019; Maithani et al., 2020).

$$L_\lambda = \text{gain} * \text{DN} + \text{bais} \tag{1}$$

where, L_λ = spectral radiance at the sensor; QCAL = quantized calibrated pixel value; gain and bias = the band specific rescaled factor (Adeyeri et al., 2017). The radiance was converted to reflectance by performing Eq. (2).

$$\rho_\lambda = \frac{L\lambda * \pi * d^2}{ESUN * \sin\theta_E} \tag{2}$$

where, ρ_λ= reflectance at ToA; d = earth-sun distance in an astronomical unit on the day of image acquisition; ESUN = the mean solar exo-atmospheric irradiance; θ_E = the solar elevation angle in degree (Adeyeri et al., 2017).

2.4. LULC classification

For image classification and visualization of different land cover classes, Landsat 5 (TM-30 m) and Landsat 8 (OLI-30 m) images were used (Ahmed et al., 2013). In the ERDAS Imagine 2014 edition, atmospheric and radiometric adjustment has been carried out and increased by applying majority filter procedures for improved image quality (Thakur et al., 2019; Mondal et al., 2021a, b). The required bands (band 1 to 5 for Landsat 5 and band 2 to 7 for Landsat 8) were composited for LULC classification. A supervised image classification process was performed in this research to determine the LULC types, as recommended by the literature (Kafy et al., 2021; Georgiana and Uriţescu, 2019). The LULC is separated into five different categories (Table 2) (built-up area-BU, bare land-BL, agricultural land-AL, waterbody-WB, and vegetation-VG) to recognize the change in land cover pattern (Georgiana and Uriţescu, 2019; Faisal et al., 2021). The elevation data was collected from the United States Geological Survey (USGS) and the Arc map 10.5 platform was used to process the elevation data. For preparing the elevation map, SRTM 30m dem was first collected and then the area of interest was extracted by using the extract by mask tool. Following the authoring, new appropriate and quantitative image grouping precision estimate approaches known as Kappa statistics and confusion matrix were developed to verify the accuracy of the arrangement (Pal and Ziaul 2017; Morshed et al., 2022). An equalized stratified random sampling method was used to generate 160 points of reference for accuracy testing. With Google Earth photos as a reference point, overall accuracy, user accuracy, and Kappa Coefficient were examined. The following Eqs. (3), (4), (5), and (6) were used to determine accuracy. All the images achieved accuracy of more than 86%.

2.5. Land use indices calculation procedure

2.5.1. Normalized difference built-up index (NDBI)

NDBI quantifies the concentration of built-up area by performing a function between the portion of near-infrared (NIR) (band 5 for Landsat 8 and band 4 for Landsat 5) and shortwave infrared (SWIR) (band 6 for Landsat 8 and band 5 for Landsat 5) refracted radiation accumulated by the Landsat Multi-spectral sensing element under the conditions (equation 7) (Zhang et al., 2013).

$$\text{NDBI} = \frac{(\text{SWIR} - \text{NIR})}{(\text{SWIR} + \text{NIR})} \tag{7}$$

NDBI values range from -1 to 1. The higher the value, the more developed area and construction land, metro area, or created territory exists. Consequently, the lower the value, the less built-up area, rural region, or undeveloped terrain exists (Kafy et al., 2021).

2.5.2. Modified Normalized Difference Water Index (MNDWI)

The NDWI is a spatial indicator that responds to changes in leaf moisture content (Das et al., 2021). NDWI is calculated using the following Eq. (8).

$$\text{NDWI} = \frac{(\text{Green} - \text{NIR})}{(\text{Green} + \text{NIR})} \tag{8}$$

However, MNDWI is a modified NDWI that has been used in this study. For the enhancement of open water features, the MNDWI employs pixel values from green (band 3 for Landsat 8 and band 2 for Landsat 5) and short-wave infrared (SWIR) bands (band 6 for Landsat 8 and band 5 for Landsat 5). It also reduces built-up area characteristics that are commonly linked to water in other indexes. The MNDWI estimation ranges from -1.0 to +1.0. Calculation of Modified MNDWI is calculated using Eq. (9).

$$\text{MNDWI} = \frac{(\text{Green} - \text{SWIR})}{(\text{Green} + \text{SWIR})} \tag{9}$$

2.5.3. Normalized Difference Bareness Index (NDBaI)

NDBaI was suggested by Chen et al. (2006) to distinguish bare land from other land uses (NDBaI). NDBaI has already been used multiple

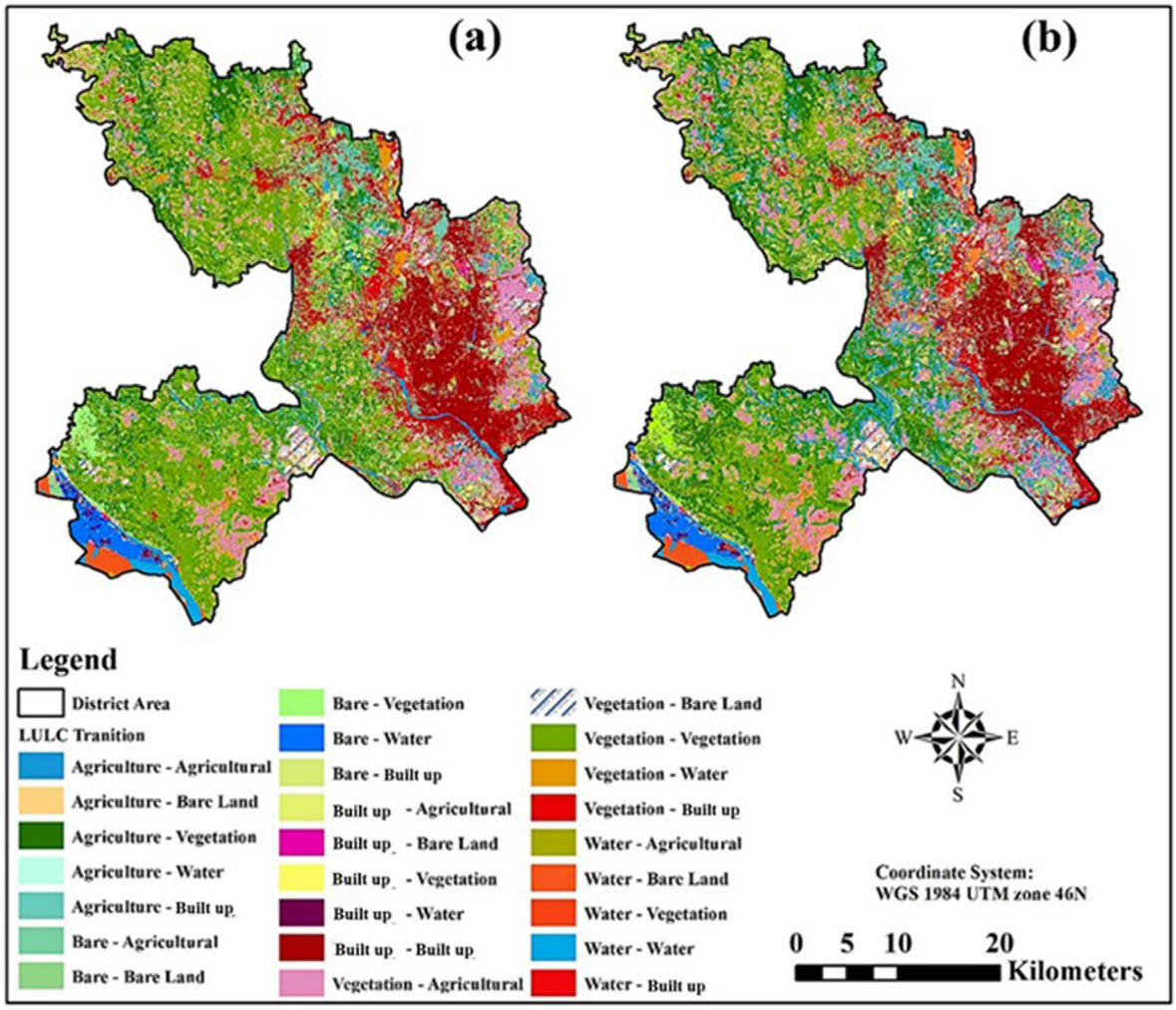

Figure 4. LULC transition matrix of Dhaka district (a) summer (b) Winter during 2000–2020.

times in recent studies to estimate vegetation cover. The range of the NDBaI estimation is -1.0 to +1.0. The NDBaI is calculated using Eq. (10) following the research of (Imran et al., 2021).

$$\text{NDBaI} = \frac{((\text{SWIR Band1} - \text{TIRS Band 1}))}{(\text{SWIR Band1} + \text{TIRS Band 1})} \quad (10)$$

where, TIRS 1 (band 10 for Landsat 8 and band 6 for Landsat 5) is the Thermal Infrared Sensor band 1 and SWIR 1 is the Short-wave infrared band 1 (band 6 for Landsat 8 and band 5 for Landsat 5).

2.5.4. Normalized difference vegetation index (NDVI)

Pixel values from the Landsat Near-Infrared (band 5 for Landsat 8 and band 4 for Landsat 7) and Red (band 4 for Landsat 8 and band 3 for Landsat 5 image) spectral bands are employed to identify the NDVI (Georgiana and Uritescu, 2019; Zhang et al., 2016). NDVI is calculated as given below (equation 11):

$$\text{NDVI} = \frac{(\text{NIR Band} - \text{Red Band})}{(\text{NIR Band} + \text{Red Band})} \quad (11)$$

To identify the difference in land cover during the assessment period, the NDVI was analyzed in real time. The NDVI ranges from -1.0 (lowest) to +1.0 (highest). Low NDVI values are associated with rock land or metropolitan areas as well as developed areas. Table 3 represents the NDVI value ranges for different LULC types.

2.6. Land surface temperature (LST) calculation process

LST is the radioactive temperature of earth surface which is critical for understanding the basic science of the land surface via the energy cycle and aquatic exchange with the environment (Zhang et al., 2013; Ahmed et al., 2013). LST analysis using satellite thermal data entails a variety of procedures, including sensor radiometric alignment, correction of air and surface reflectance and spatial variation of LULC. For calculating LST thermal band 11 (for Landsat 8) and thermal band 6 (for Landsat 5) were utilized. The process of calculating LST is explained below by following the method of Thakur et al. (2020a, b) and Kafy et al. (2021) (Eqs. (12), (13), (14), (15), and (16)):

$$L\lambda = A_L + M_L \times QCAL \quad (12)$$

where, $L\lambda$ = TOA Spectral Radiance ($W/(m^2 \times sr \times \mu m)$); M_L = Radiance multiplicative scaling factor for the band;

A_L = Band's Radiance additive scaling factor; QCAL = Digital Numbers (DN) of band 10.

After that, TOA spectral radiance ($L\lambda$) values are converted into At-Satellite Brightness Temperature (TB).

$$TB = \frac{\sum(K_2)}{(ln(K1/L\lambda + 1)} \quad (13)$$

where, TB = At-Satellite Brightness Temperature, in Kelvin (K); K1, K2 = Thermal conversion constants for the band.

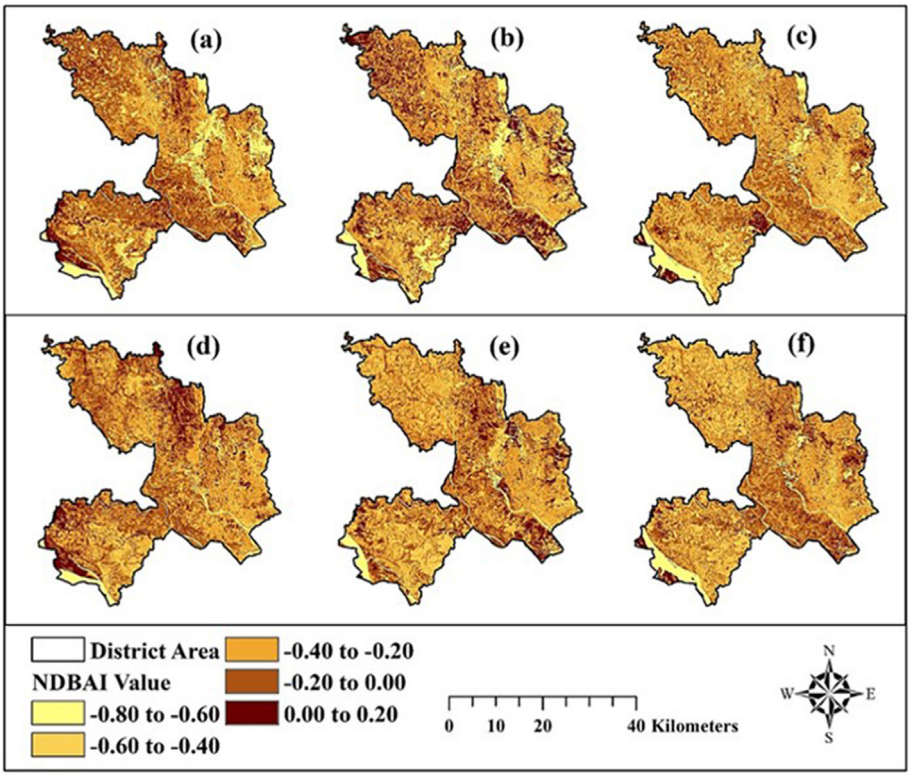

Figure 5. NDBAI profile of the study area during winter season of (a) 2000 (b) 2010 (c) 2020 and summer season of (d) 2000 (e) 2010 (f) 2020.

Then, Proportion of vegetation cover (PV) and surface emissivity (ε) is calculated according to equation as below (equation 14 &15)-

$$Pv = \left[\frac{(\text{NDVI} - \text{NDVImin})}{(\text{NDVImax} - \text{NDVImin})}\right]^2 \tag{14}$$

$$\varepsilon = (0.004 \times \text{Pv}) + 0.986 \tag{15}$$

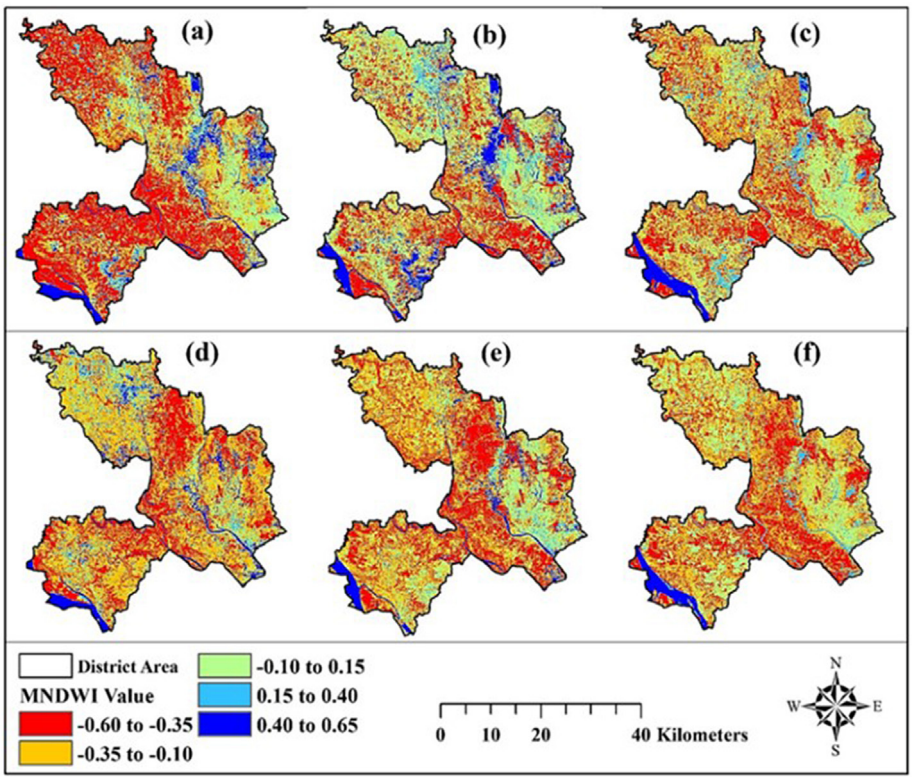

Figure 6. MNDWI profile of the study area during winter season of (a) 2000 (b) 2010 (c) 2020 and summer season of (d) 2000 (e) 2010 (f) 2020.

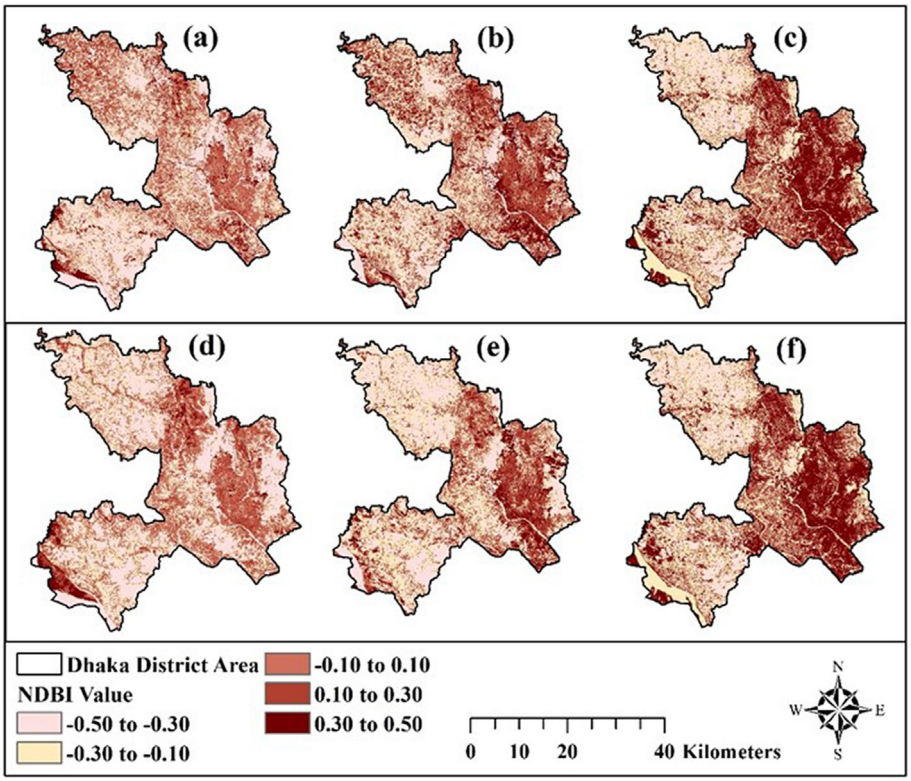

Figure 7. NDBI profile of the study area during winter season of (a) 2000 (b) 2010 (c) 2020 and summer season of (d) 2000 (e) 2010 (f) 2020.

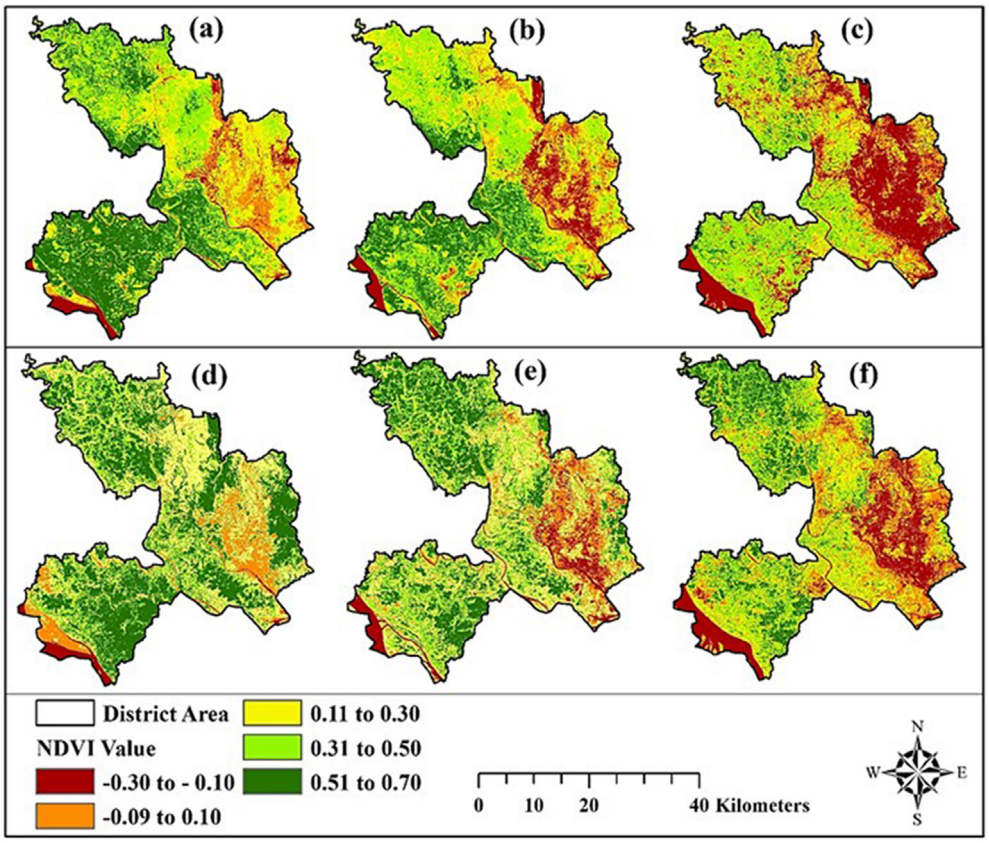

Figure 8. NDVI profile of the study area during winter season of (a) 2000 (b) 2010 (c) 2020 and summer season of (d) 2000 (e) 2010 (f) 2020.

Table 6. Percentage of areas under different ranges of land use indices.

	2000		2010		2020	
NDBAI	Winter	Summer	Winter	Summer	Winter	Summer
-0.80 to -0.60	9.96	5.96	8.03	5.26	9.75	4.05
-0.60 to -0.40	7.75	8.75	22.9	22.9	26.11	35.11
-0.40 to -0.20	32.03	32.97	26.55	31.65	24.4	23.9
-0.20 to 0.00	32.98	33.41	22.16	24.56	32.41	25.41
0.00 to 0.20	17.28	18.91	20.36	15.63	7.33	11.53
MNDWI						
-0.60 to -0.35	44.32	32.32	22.63	34.63	19.62	38.59
-0.35 to -0.10	19.33	27.33	32.96	29.96	30.65	25.41
-0.10 to 0.15	26.38	33.67	35.55	27.55	35.52	26.69
0.15 to .40	2.75	2.62	2.85	2.9	6.75	3.75
0.40 to 0.64	7.22	4.06	6.01	4.96	7.46	5.56
NDBI						
-0.50 to -0.30	36.98	36.96	24.18	32.03	28.75	33.75
-0.30 to -0.10	11.89	17.81	25.95	16.55	15.07	13.15
-0.10 to 0.10	15.1	12.15	10.45	10.45	8.34	7.34
0.10 to 0.30	29.8	25.8	25.62	26.62	13.43	10.43
0.30 to 0.50	6.23	7.28	13.8	14.35	34.41	35.33
NDVI						
-0.30 to -0.10	5.6	3.93	14.45	9.8	25.75	19.47
-0.09 to 0.10	23.5	20.17	7.6	8.41	9.41	14.35
0.11 to .30	12.8	15.8	10.8	11.03	7.69	6.52
0.31 to 0.50	20.65	19.65	34.65	33.6	26.65	28.65
0.51 to 0.70	37.45	40.45	32.5	37.16	30.5	31.01

Lastly, the TOA Brightness Temperature was converted to LST values in Kelvin (K).

$$LST = \left[\frac{TB}{1 + \left(\frac{\lambda \times TB}{\alpha}\right)\ln\varepsilon}\right] \quad (16)$$

where

λ = the wavelength of emitted radiance
α = hc/k (1.438×10^{-2} mK)
h = Planck constant (6.626×10^{-34} J s-1)
c = velocity of light (2.998×10^{8} m s^{-1})
k = Boltzmann constant (1.38×10^{-23} J/K)

2.7. Correlation analysis

To determine the interlinkage between two different variables or variable of interest correlation analysis is very effective (Obilor and Amadi, 2018; Sedgwick, 2014). So, for assessing the nexus between land use indices and LST, regression models namely linear regression, Pearson's correlation coefficient (Pr) was calculated using: x_i = values of the x-variable in a sample, x' = mean of the values of the x-variable y_i = values of the y-variable in a sample and y' = mean of the values of the y-variable (equation 17) (Obilor and Amadi, 2018).

$$Pr = \frac{\sum (x_i - x')(y_i - y')}{\sqrt{\sum (x_i - x')^2 \times (y_i - y')^2}} \quad (17)$$

Spearman's rank correlation coefficient (SC) (Sedgwick, 2014) was also calculated for all the seasons and years. Where d_i = difference between the two ranks of each observation, n = number of observations (equation 18).

$$SC = 1 - \frac{6\sum d_i^2}{n(n^2 - 1)} \quad (18)$$

3. Results

3.1. Seasonal variability of LULC distribution between 2000 and 2020

The outcome of the supervised image classifications is presented in Figure 2 and the statistics of the classified LULC types for both the summer and winter seasons (area in %) and change (in km^2) are presented in Table 4. Figure 3 shows the LULC variation ranges (standard deviations) for summer and winter season. The LULC analysis shows that, in 2000, the vegetation (VG) covered the largest areas, accounting for 48.14% in winter and 49.14% in summer.

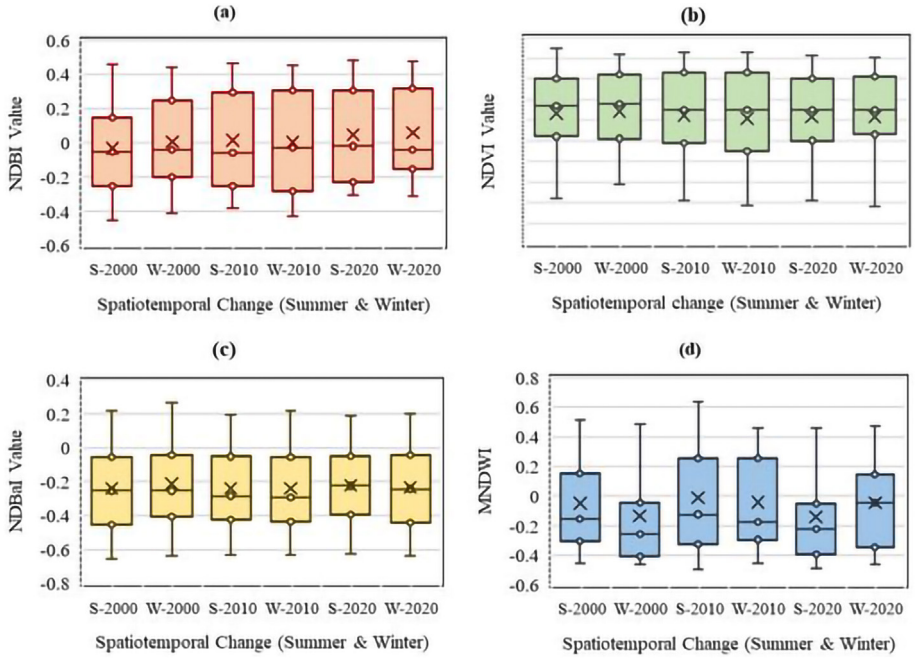

Figure 9. Min, max and mean value for NDBI, NDVI, NDBAI, MNDWI of 2000, 2010 & 2020.

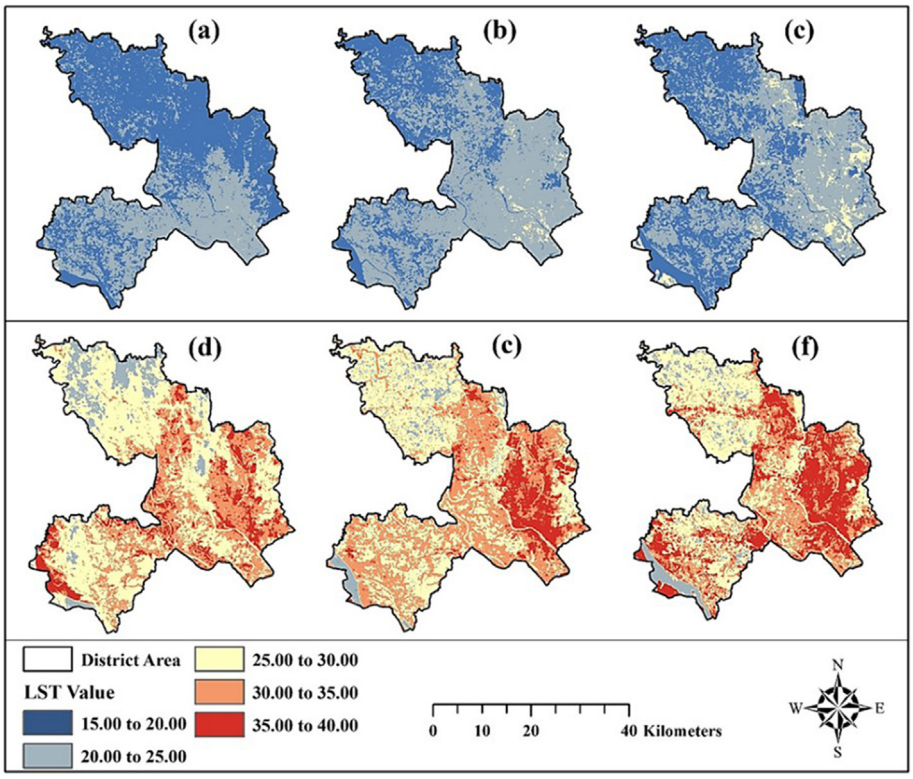

Figure 10. Derived LST profile of the study area during winter season of (a) 2000 (b) 2010 (c) 2020 and summer season of (d) 2000 (e) 2010 (f) 2020.

The second largest, the agricultural land (AL), covered 23.37% of areas in winter and 24.19% in summer. Water body (WB) cover was the lowest (4.57% in winter and 4.43% in summer). Rapid population growth, higher urbanization and migration rates, and the transformation of other LULC types into built-up areas have all increased over the last two decades. In 2020, the built up (BU) cover was the second largest, increasing by 126.97 km^2 (59.40%) during 2000–2020. About 27.24% (95.13 km^2) of agricultural AG covers declined, while VG covers decreased by 66.57 km^2 (8.76%) (Table 5).

Table 5 represent the seasonal LULC transformation matrix of the study area during 2000–2020. The data in Table 5 shows the considerable increase in built-up areas (103.21 km^2 from VG, 15.14 km^2 from WB, 49.6.3 km^2 from BL and 93.66 km^2 from AL). Again, a large portion of VG (195.46 km^2) was transformed into AL. The conversion of VG, AL and WB to BL was also significant (Figure 4). Dhaka is the capital city and the most advanced city in Bangladesh with the most employment and service facilities. Factors like migration from better living standards, unplanned urbanization, higher population density and increasing rates and unplanned urban expansions are responsible for the notable transformation of VG and AL in Dhaka. Such increase in built-up area is responsible for unplanned LULC transformation which led to an increase in LST and decrease in the environmental sustainability of Dhaka district.

Table 7. Observed seasonal LST variations during the study period.

LST ranges	2000		2010		2020	
	Winter	Summer	Winter	Summer	Winter	Summer
15–20 °C	61.48	0	30.21	0	42.60	0
20–25 °C	38.02	7.85	68.50	6.40	52.85	9.35
25–30 °C	0.50	51.15	1.29	33.35	4.55	33.65
30–35 °C	0	28.50	0	41.00	0	20.50
35–40 °C	0	12.50	0	19.25	0	36.50

The results of the LULC types evaluated in Table 4 show that the overall percentage and total area of the water body have increased over time. But previous research findings, for example, Imran et al. (2021), Kafy et al. (2021), and Moniruzzaman et al. (2021) suggest that water bodies have decreased and small water bodies have turned into built-up areas or other types of land cover over time in Dhaka city and surrounding areas. The analysis results of the present study show such results because the study area is on the bank of the Padma River, which is one of the largest rivers in Bangladesh. Over the past few decades, the Padma River has changed its tidal flow, resulting in river erosion and several river training works taking place (CEGIS, 2005; Neill et al., 2010; Hassan and Akhtaruzzaman, 2010; Ophra et al., 2018). However, the transformation of water bodies into built-up land or other land cover types (vegetation, agricultural, bare land) can be better understood by observing the LULC transition matrix (Table 5).

3.2. Seasonal variability and intensity of land use index analysis, 2000–2020

For both the winter and summer season, the health status of built-up areas, bare land, soil moisture and vegetation in the study area were measured using the NDBAI, MNDWI, NDBI, and NDVI indices, respectively. The outcomes of these indices are presented in Figures 5, 6, 7, and 8. The value range of each index is divided into five groups, and the area of each group (area in %) of all the indices is presented in Table 6. The details seasonal statistics of the land-use indices are presented in Figure 9.

3.3. Seasonal variability of LST, 2000–2020

Figure 10 represents the (a–c) winter season and (d – f) summer season LST of the study area during 2000–2020. Table 7 shows the areas (in percentage) witnessed different LST values over the study period. The seasonal outcomes of the LST analysis shows a huge variation in summer and winter. Figure 10 shows the land covers of the study area witnessed

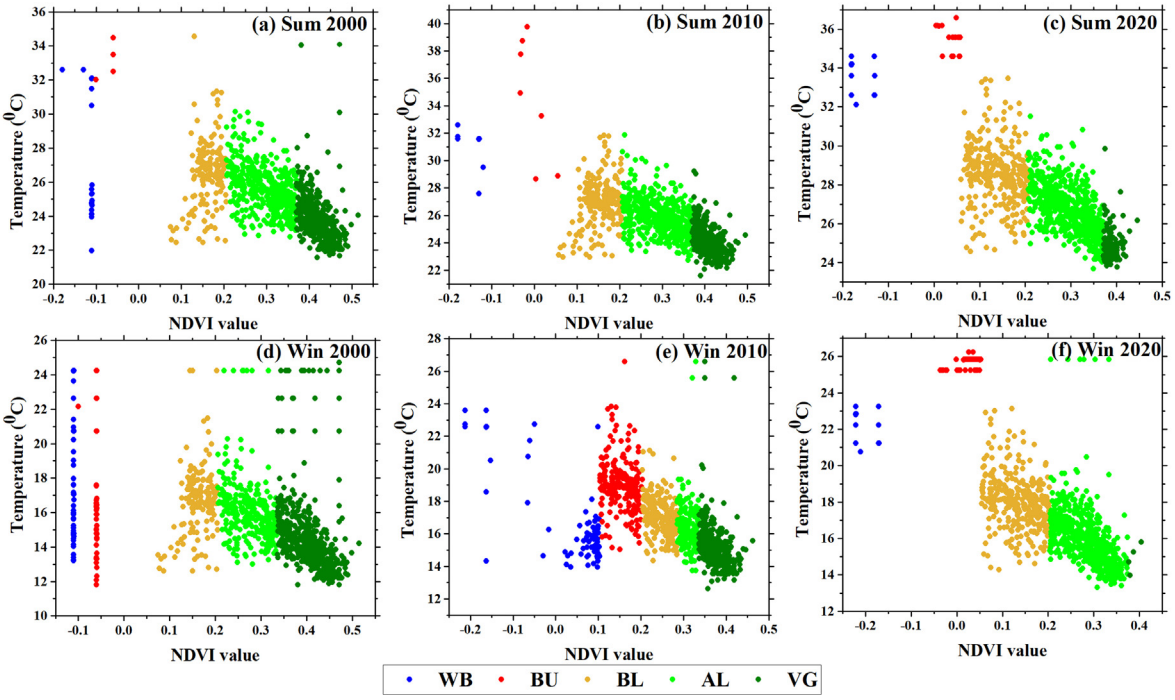

Figure 11. Distributions of LST in different LULC types.

Table 8. Derived average LST in different LULC types.

	Years	WB	BU	BL	AL	VG
Summer	2000	30.93	33.73	26.81	25.57	23.84
	2010	31.38	34.95	26.93	25.79	24.26
	2020	33.36	35.49	28.54	26.76	24.98
Winter	2000	20.81	20.04	16.71	16.06	14.8
	2010	19.94	20.11	17.01	16.73	15.92
	2020	21.88	25.72	18.01	16.95	14.94

an increasing trend of LST over the study period (2000–2020). The winter season LST range was observed between 11.81 °C–24.71 °C in 2000, 12.62 °C–26.89 °C in 2010 and 13.31 °C–26.24 °C in 2020. The mean winter season LST was observed 17.30 °C, 18.64 °C and 19.91 °C, respectively in 2000, 2010 and 2020. The mean LST for summer season was found to be more than 10 °C than the mean LST in winter season (27.74 °C, 28.81 °C and 30.74 °C in three distinct years). The summer season LST ranged from 27.56 °C to 34.59 °C in 2000, 21.62 °C–32.65 °C in 2010, and 23.66 °C–37.66 °C in 2020.

The statistics of spatial distributions of the LST are presented in Table 7. Analysis shows that 61.48% of areas LST was between 15 °C–20 °C during winter in 2000, whereas it decreased to 42.60% in winter 2020. In winter 2000, about 0.50 of total areas LST was above 25 °C, and in winter 2020, about 4.55% of areas LST was observed above 25 °C. Substantial change in LST was also observed for the summer season also. In summer 2000, about 12.50% of areas exhibited LST above 35 °C, this percentage increased to 19.25% in summer 2010 and to 36.50% in summer 2020. Figure 10 shows that the increasing trend of LST was scattered throughout the district, but increased mostly in Dhaka Metropolitan area. The regions that exhibited LST between 25 °C–30 °C were distributed mostly in the suburban regions of Dhaka district, with areas of 51.15% in 2000, 33.35% in 2010, and 33.65% in 2020.

3.4. Nexus between LULC and LST

3.4.1. Distribution of LST under different LULC types

To assess the dynamics of LST in different LULC classes, we randomly selected 1250 points, and extracted the LST, NDVI, NDBAI, NDBI, and MNDWI values of these points. Figure 11 represents the distributions of LST in different LULC classes, which were classified based on the NDVI value ranges. Table 8 shows the observed mean LST in different LULC classes over the study period. In accordance with Table 8, in summer 2000, the highest mean LST was observed 33.73 °C in BU, and lowest in VG cover. The BU cover areas had the highest average LST in both seasons, followed by WB, BL, AL and VG. The highest mean LST was observed 35.49 °C in summer 2020, followed by 34.95 °C in summer 2010 and 33.73 °C in summer 2000.

Figure 11 shows that the LST in some VG covers was also high in 2000 (in both seasons) and in winter 2010, and we also observed high LST in BL and AL in all the seasons. The average LST in all the LULC has increased over the courseof the investigation. Analysis shows that the minimum average LST was observed in VG cover in both seasons over the study period. This is because vegetation cover provides shade and helps evapotranspiration, which lowers the temperature. Also, sequestration of CO_2 by vegetation reduces temperature. Although the mean differences between the LST in BU and WB are small, between BU and other three land covers were very high in both seasons, especially between the BU and VG was more than 9 °C.

3.5. Regression analysis

In this section, we assessed the nexus between the seasonal LST and land use indices by using the linear regression model, Pearson's correlation model, and Spearman's rank correlation method. Figure 12 and Figure 13 represent the outcomes of the regression analysis for the summer season and winter season, respectively.

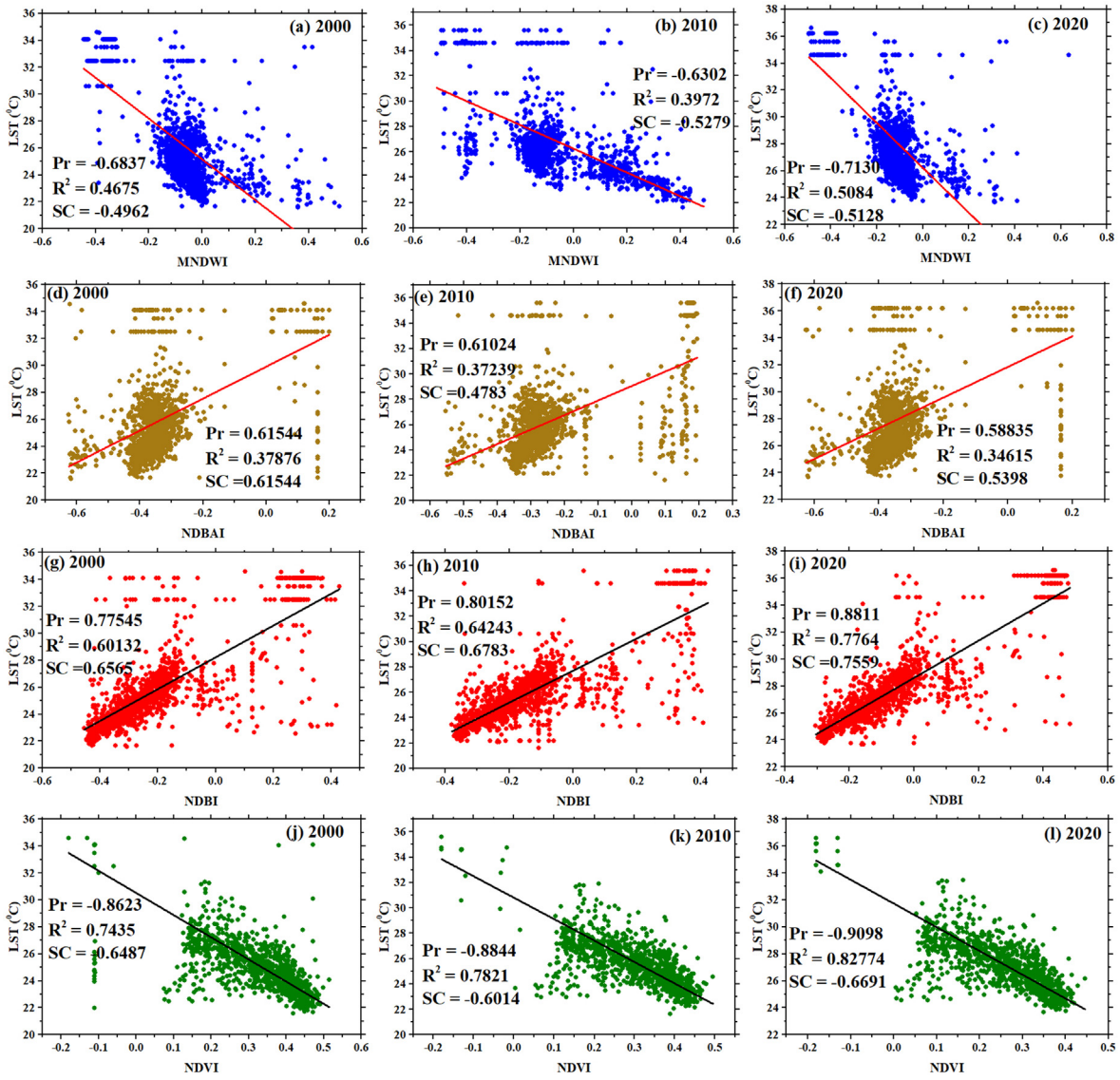

Figure 12. Correlation between the summer season land use indices and LST during 2000–2020.

Among the land use indices, MNDWI (Fig. 12a–c, Fig. 13a–c) and NDVI (Fig. 12j–l, Fig. 13j–l) showed inverse correlations, while NDBI (Fig. 12g–i, Fig. 13g–i) and NDBAI (Fig. 12d–f, Fig. 13d–f) showed positive correlations. Among the land use indices, the NDVI had the maximum correlation value in both seasons.

The R^2 value for NDVI vs LST is 0.7435, 0.7821 and 0.82774, respectively; and Pearson's r were -0.8623, -0.8844 and -0.9098, respectively in the years 2000, 2010 and 2020 indicates the strong negative correlation between the LST and vegetation health dynamics. The Pearson's correlation coefficient values of -0.6837, -0.6302 and -0.7130 indicate strong negative correlation between LST and water health during the summer season. For NDBI vs LST, the summer season LST value was calculated 0.60132, 0.64243 and 0.7764, respectively, which indicates strong positive correlations between built-up expansion and LST. The linear regression, Spearman correlation coefficients and Pearson's coefficients demonstrate that the increase in LST in Dhaka district was mostly influenced by the decline of vegetation and increase in built-up areas.

Figure 13 shows that all the land cover dynamics have significant influences on the LST dynamics during the winter season. The Spearman coefficient values -0.5005, -0.4540 and -0.4640 (Pearson's r = -0.5196, -0.450, -0.4944) for the years 2000, 2010 and 2020 indicate moderate negative correlations between MNDWI and LST dynamics. The correlation coefficient between NDVI and LST also indicates strong negative influences on LST dynamics. Previous studies have confirmed the significant inverse influences of water and vegetation dynamics on surface temperature (Zhi et al., 2020). The positive correlations between the NDBAI and LST (Pearson's r = +0.4643, +0.4899 and +0.47701) indicate that the increase of bare lands has been accelerating the surface temperature of Dhaka. Transformations of AL and VG to bare lands decrease the soil's heat absorption capacity and thus increase the surface temperature. On the other hand, increase of the built-up areas helped to accelerate the average LST of Dhaka district significantly. This is reflected in the association between NDBI and LST. The R^2 value between both seasons' NDBI and LST shows the positive significant influences of the built-up expansions on the rise of LST in the study area. Imran et al. (2021) found that the NDBI and NDBI are positively correlated with LST dynamics of Dhaka Metropolitan area, while NDVI is negatively correlated.

4. Discussion

This research quantifies the nexus between seasonal diversity of LULC indices and LST in Dhaka district of Bangladesh for the period

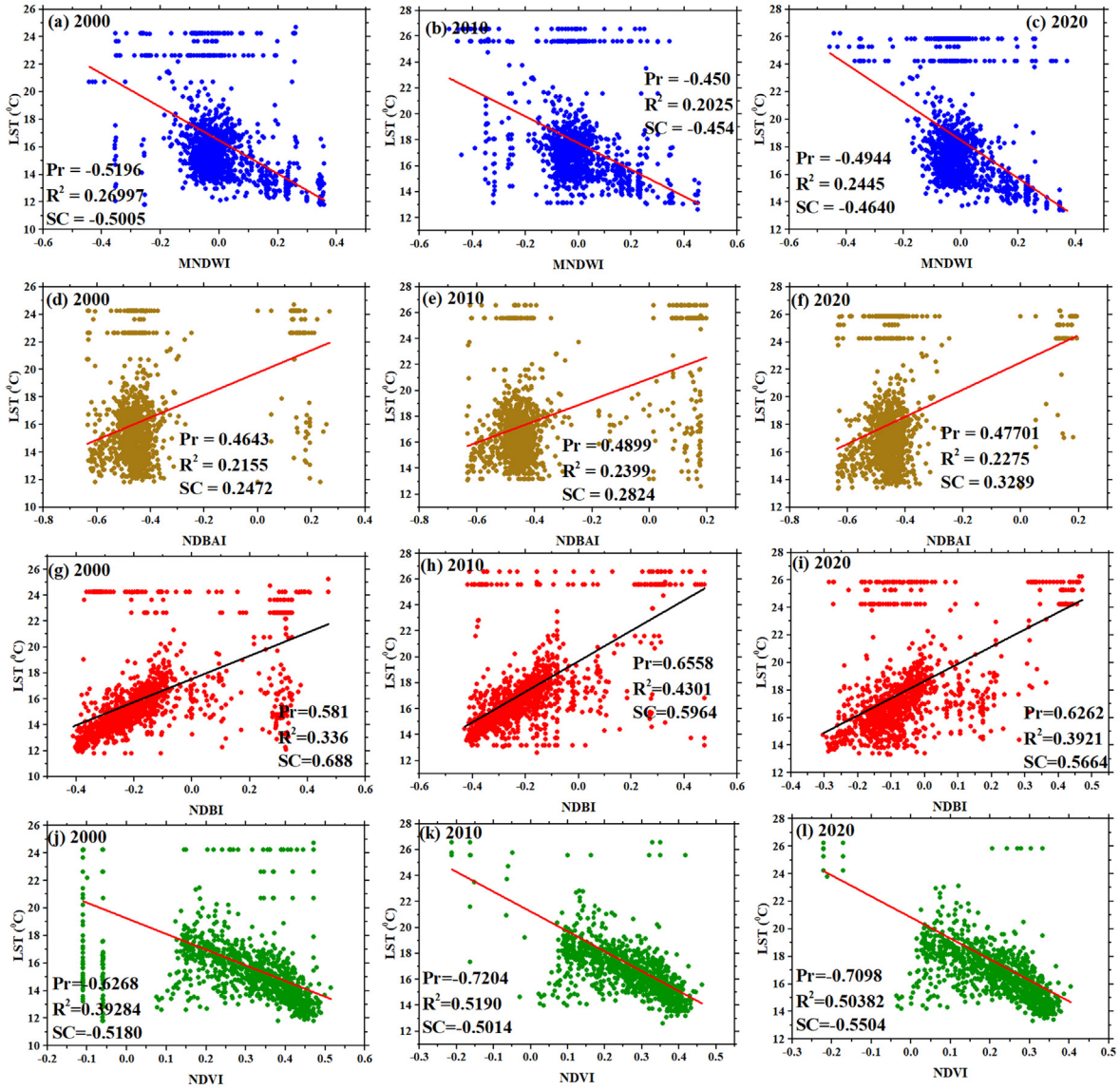

Figure 13. Correlation between the winter season land use indices and LST during 2000–2020.

between 2000 and 2020. The population of Dhaka district increased from 10.285 million to 12.04 million between 2000 and 2011. In 2011, the population density of Dhaka district was 8229 people per sq. km., whereas it was 30551 per km^2 in the Dhaka Metropolitan area (Faisal et al., 2021). This higher population increase in Dhaka witnessed a substantial decline of AL and VG in the study area. A large portion of the AL and VG covers have slightly disappeared and transformed into built-up covers. The outputs show that LST increased over the last 20 years significantly; in the summer of 2000, around 12.50 percent of places had LSTs exceeding 350 degrees Celsius. This number grew to 19.25 % in the summer of 2010 and to 36.50 % in the summer of 2020. Similar seasonal variation was observed by (Mallick, 2021) in India. A comparable result was also reported by Kafy et al. (2021) in Comilla, Bangladesh. However, the mean LST of WB was observed relatively high in this study, the direct disposal of industrial wastes into river water is the possible reason behind this higher mean LST of WB (Bashar and Fung, 2020). Akter et al. (2021) observed the lowest LST in the vegetation covers and highest in the built-up areas and river side areas across the northwestern region of Bangladesh during 1990–2018.

Previous research findings suggest that water bodies have diminished and water bodies have transformed into built-up areas or other types of land cover through time in Dhaka city and neighboring areas, according to Imran et al. (2021), Kafy et al. (2021), and Moniruzzaman et al. (2021). Similarly, the present study suggests that small water bodies have decreased due to excessive urbanization (Figure 4 & Table 5). But this study shows the overall percentage of water bodies has increased over the past few decades (Table 4). The reason behind such findings is the Padma River, alongside Dhaka district, and the river's tidal flow has shifted, resulting in river erosion and river training projects (CEGIS, 2005; Neill et al., 2010; Hassan and Akhtaruzzaman, 2010; Ophra et al., 2018). The study area for this research includes the Padma River, which was hardly considered by other researchers. So, the findings explain that waterbodies inside Dhaka city and surrounding areas have decreased, but due to the shift in the tidal flow of the Padma River, the overall percentage of waterbodies has increased a little over time.

The results of this research indicated a substantial negative association between the LST and vegetation health trends. On the other hand, positive correlation was observed between NDBI and LST. The regression results were strong enough to justify the correlations and researchers

such as Kafy et al. (2020) and Zhang et al. (2022) also evaluated such correlation results.

Figure 2 and figure 10 clearly explains that build up area and bare land is producing more LST than other types of land cover. Urban expansion, centralization, decrease of vegetation and water bodies are particularly responsible for the increasing trend of LST. In the study of Fu and Weng (2016), Trenberth (2011) and Hassan and Southworth (2018) explained how mega urbanization, vegetation and agglomeration influences the dynamics of surface temperature. Despite the fact that the aforementioned findings are informative, they should be interpreted with caution because they were obtained from satellite images taken at various times. More in-situ data needs to be incorporated to confirm and validate the findings of this study.

5. Conclusion

LULC through increasing built-up and decreasing vegetation area is one of the most important contributors to the rising LST. Knowledge of seasonal LULC and LST dynamics has the potential to be used for mitigating LST hotspots and ensuring ecological balance for the living environment. This study explored the impacts of seasonal dynamics of land use indices on the LST between 2000 and 2020. Four land use indices – MNDWI, NDVI, NDBAI, and NDBI – were used to measure the spatial and seasonal variation of LULC and LSC in the Dhaka District of Bangladesh. The findings of this paper are as follows: First, about 126.32 km^2 of built-up area was increased in Dhaka district by replacing 96.80 km^2 of agricultural land and 63.20 km^2 of vegetation cover. The built-up areas increased rapidly in the sub-urban areas in comparison to the Dhaka city area. Second, the spatial distribution of mean summer and winter season LST in Dhaka district showed an increase of 3.07 °C and 1.89 °C, respectively. Besides, areas of higher LST (summer season) between 35^0C–40 °C increased from 12.50% to 36.50%, whereas areas of the lowest LST ranges between 15^0C–20 °C decreased from 61.48% to 42.60% over the study period. Finally, the MNDWI and NDVI indices were inversely correlated with LST dynamics, while the NDBI and NDBAI indices were positively correlated. Furthermore, the decline of vegetation cover has been identified as the most influential factor for the rise of LST in the study area.

First, 126.32 km^2 built-up area increased in Dhaka district by replacing 96.80 km^2 of agricultural land and 63.20 km^2 of vegetation cover. The built-up areas increased rapidly in the sub-urban areas in comparison to the Dhaka city area. Second, the spatial distribution of mean summer and winter season LST in Dhaka district showed an increase of 3.07 °C and 1.89 °C, respectively. Besides, areas of higher LST (summer season) between 35^0C–40 °C increased from 12.50% to 36.50%, whereas areas of the lowest LST ranges between 15^0C–20 °C decreased from 61.48% to 42.60% over the study period. Finally, the MNDWI and NDVI indices were inversely correlated with LST dynamics, while the NDBI and NDBAI indices were positively correlated. Furthermore, the decline of vegetation cover has been identified as the most influential factor for the rise of LST in the study area.

The study has several limitations. First, freely available low-resolution images were used for the study. Secondly, remote sensing techniques on low-resolution images covering vast areas result in limited accuracy. Therefore, we have very little justification for the increase in waterbody area over the study period. However, the methodological approach of this study proposes a low-cost and efficient method for continuous monitoring of LULC and LST. Therefore, land use planners and urban managers can continuously monitor the LULC and LST change patterns and employ subsequent mitigating as well as policy measures for guiding land development.

Declarations

Author contribution statement

Mizbah Ahmed Sresto; Sharmin Siddika: Conceived and designed the experiments; Performed the experiments.

Md. Abdul Fattah; Syed Riad Morshed: Analyzed and interpreted the data; Wrote the paper.

Md. Manjur Morshed: Contributed reagents, materials, analysis tools or data; Wrote the paper.

Funding statement

This research did not receive any specific grant from funding agencies in the public, commercial, or not-for-profit sectors.

Data availability statement

No data was used for the research described in the article.

Declaration of interest's statement

The authors declare no conflict of interest.

Additional information

No additional information is available for this paper.

References

Abir, F.A., Saha, R., 2021. Assessment of land surface temperature and land cover variability during winter: A spatio-temporal analysis of Pabna municipality in Bangladesh. Environ. Chall. 4, 1–12.

Adeyeri, O.E., Akinsanola, A.A., Ishola, K.A., 2017. Investigating surface urban heat island characteristics over Abuja, Nigeria: relationship. Remote Sens. Appl. Soc. Environ. 7, 57–68.

Ahmed, B., Kamruzzaman, M., Zhu, X., Rahman, M.S., Choi, K., 2013. Simulating land cover changes and their impacts on land surface temperature in Dhaka, Bangladesh. Rem. Sens. 5, 5969–5998.

Akbar, T.A., Hassan, Q.K., Ishaq, S., Batool, M., Butt, H.J., Jabbar, H., 2019. Investigative spatial distribution and modelling of existing and future urban land changes and its impact on urbanization and economy. Rem. Sens. 11 (2), 105.

Akram, W.S.K., Mondal, I., Bandyopadhyay, J., 2018. Crop Suitability Analysis in Water Resource Management of Paschim Midnapore District: a Remote Sensing Approach, Sustainable Water Resources Management, 5. Springer, pp. 797–815.

Akter, Tanzida, Gazi, Md. Yousuf, Mia, Md. Bodruddoza, 2021. Assessment of land cover dynamics, land surface temperature, and heat island growth in Northwestern Bangladesh using satellite imagery. Environmental Processes 8, 661–690.

Al-Hameedi, W.M.M., Chen, J., Faichia, C., Al-Shaibah, B., Nath, B., Kafy, A.-A., Hu, G., Al-Aizari, A., 2021. Remote sensing-based urban sprawl modeling using multilayer perceptron neural network Markov chain in Baghdad, Iraq. Rem. Sens. 13, 4034.

Arefin, S., Rashid, T., Habib, D., 2019. Infrastructural development and vulnerabilities: a sociological study of two selected flyovers in Dhaka city, Bangladesh. Open J. Soc. Sci. 7, 18–29.

Bangladesh Bureau of Statistics (BBS), 2017. Report on CWS 2016 Urban Areas in Bangladesh. Ministry of Planning, Dhaka.

Bashar, Toriqul, Fung, Ivan W.H., 2020. Water pollution in a densely populated megapolis, Dhaka. Water 12, 2124.

Begum, M., Bala, S., Islam, A., Islam, G., Roy, D., 2021. An analysis of spatio-temporal trends of land surface temperature in the Dhaka metropolitan area by applying landsat images. J. Geogr. Inf. Syst. 13, 538–560.

CEGIS, 2005. Prediction for Bank Erosion and Morphological Changes of the Jamuna and Padma River. Center for Environmental and Geographic Information Services (CEGIS), Dhaka.

Chen, X.L., Zhao, H.M., Li, P.X., Yin, Z.Y., 2006. Remote sensing imagebased analysis of the relationship between urban heat island and land use/cover changes. Remote Sens. Environ. 104 (2), 133–146.

Das, N., Mondal, P., Sutradhar, S., Ghosh, R., 2021. Assessment of variation of land use/land cover and its impact on land surface temperature of Asansol subdivision. Egyptian J. Rem. Sens. Space Sci. 24 (1), 131–149.

Dhar, R.B., Chakraborty, S., Chattopadhyay, R., Sikdar, P.K., 2019. Impact of land-use/land-cover change on land surface temperature using satellite data: a case study of rajarhat block, north 24-parganas district, West Bengal. J. Indian Soc. Rem. Sens. 47, 331–348.

Faisal, A.-A., Kafy, A.-A., Rakib, A.A., et al., 2021. Assessing and predicting land use/land cover, land surface temperature and urban thermal field variance index using Landsat imagery for Dhaka Metropolitan area. Environ. Chall. 4 (100192).

Fattah, M., Morshed, S.R., Morshed, S.Y., 2021a. Impacts of land use-based carbon emission pattern on surface temperature dynamics: experience from the urban and suburban areas of Khulna, Bangladesh. Remote Sens. Appl. Soc. Environ. 22, 100508.

Fattah, M., Morshed, S.R., Morshed, S.Y., 2021b. Multi-layer perceptron-Markov chain-based artificial neural network for modelling future land-specific carbon emission pattern and its influences on surface temperature. SN Appl. Sci. 3, 359.

Fattah, M., Morshed, S.R., 2022. Assessment of the responses of spatiotemporal vegetation changes to climatic variability in Bangladesh. Theor. Appl. Climatol. 148, 285–301.
Fu, P., Weng, Q., 2016. A time series analysis of urbanization induced land use and land cover change and its impact on land surface temperature with Landsat imagery. Rem. Sens. Environ. 17, 205–214.
Gazi, A., Mondal, I., 2018. Urban heat island and its effect on dweller of Kolkata metropolitan area using geospatial techniques. Int. J. Comput. Sci. Eng. 6 (10), 778–794.
Gazi, Md. Yousuf, Rahman, Md Zillur, Uddin, Md. Mahin, Rahman, F.M. Arifur, 2021. Spatio-temporal dynamic land cover changes and their impacts on the urban thermal environment in the Chittagong metropolitan area, Bangladesh. GeoJournal 86 (11).
Georgiana, G., Urițescu, B., 2019. Land use/land cover changes dynamics and their effects on surface urban heat island in Bucharest, Romania. Int. J. Appl. Earth Obs. Geoinf. 80, 115–126.
Hassan, M.M., Southworth, J., 2018. Analyzing land cover change and urban growth trajectories of the mega-urban region of Dhaka using remotely sensed data and an ensemble classifier. Sustainability 10, 10.
Hassan, S., Akhtaruzzaman, A.F.M., 2010. Environmental change detection of the Padma River in the North-Western part of Bangladesh using multi-date landsat data. In: Proceedings of International Conference on Environmental Aspects of Bangladesh (ICEAB10), Japan, Sept 2010.
Huang, G.L., Cadenasso, M.L., 2016. People, landscape, and urban heat island: dynamics among neighborhood social conditions, land cover and surface temperatures. Landsc. Ecol. 31, 2507–2515.
Imran, H.M., Hossain, A., Islam, A.K.M.S., et al., 2021. Impact of land cover changes on land surface temperature and human thermal comfort in Dhaka city of Bangladesh. Earth Syst. Environ. 5, 667–693.
Kafy, A.A., et al., 2021. Impact of Vegetation Cover Loss on Surface Temperature and Carbon Emission in a Fastest-Growing City, Cumilla, Bangladesh, 207. Building and Environment.
Kafy, A.A., et al., 2022. Predicting the Impacts of Land Use/land Cover Changes on Seasonal Urban thermal Characteristics Using Machine Learning Algorithms, 217. Building and Environment.
Kafy, A.-A., Rahman, Md. Shahinoor, Faisal, Abdullah-Al, Hasan, Mohammad Mahmudul, Islam, Muhaiminul, 2020. Modelling future land use land cover changes and their impacts on land surface temperatures in Rajshahi, Bangladesh. Rem. Sens. Appl.: Soc. Environ. 18 (2).
Kumar, M., Mondal, I., Pham, Q.B., 2021. Monitoring Forest Landcover Changes in the Eastern Sundarban of Bangladesh from 1989 to 2019. Acta Geophys, 69. Springer, 561577.
Lemonsu, A., Kounkou-Arnaud, R., Desplat, J., Salagnac, J.-L., Masson, V., 2013. Evolution of the Parisian urban climate under a global changing climate. Clim. Chang. 116, 679–692.
Li, X., Zhou, Y., Asrar, G.R., Imhoff, M., Li, X., 2017. The surface urban heat island response to urban expansion: a panel analysis for the conterminous United States. Sci. Total Environ. 605, 426–435.
Lowe, S.A., 2016. An energy and mortality impact assessment of the urban heat island in the US. Environ. Impact Assess. Rev. 56, 139–144.
Maithani, S., Nautiyal, G., Sharma, A., 2020. Investigating the effect of lockdown during COVID-19 on land surface temperature: study of Dehradun city, India. J. Indian Soc. Rem. Sens. 48, 1297–1311.
Mallick, Javed, 2021. Evaluation of seasonal characteristics of land surface temperature with NDVI and population density. Pol. J. Environ. Stud. 30 (4).
McGee, Terry., 2006. Urbanization Takes on New Dimensions in Asia's Population Giants. Population Reference Bureau, Washington, DC.
Mondal, I., Maity, S., Das, B., Bandyopadhyay, J., Mondal, A.K., 2016. Modeling of Environmental Impact Assessment of Kolaghat thermal Power Plant Area, West Bengal, Using Remote Sensing and GIS Techniques, Modeling Earth Systems and Environment. Springer, pp. 2363–6211.
Mondal, I., Thakur, S., Ghosh, P.B., De, T.K., 2021a. Assessing the Impacts of Global Sea level rise (SLR) on the Mangrove Forests of Indian Sundarbans using Geospatial Technology, Geographic Information Science for Land Resource Management, 11. Wiley, pp. 209–228.
Mondal, I., Thakur, S., Ghosh, P.B., De, T.K., Bandyopadhyay, J., 2018. Land use/land cover modeling of sagar island, India using remote sensing and GIS techniques. In: Springer Advances in Intelligent Systems and Computing (AISC), Emerging Technologies in Data Mining and information Security, 755, pp. 771–785.
Mondal, I., Thakur, S., De, A., De, T.K., 2022. Application of the METRIC model for mapping evapotranspiration over the sundarban biosphere reserve, India. Ecol. Indicat. 136, 108553. Elsevier.
Mondal, I., Thakur, S., Juliev, M., De, T.K., 2021b. Comparative analysis of forest canopy mapping methods for the Sundarban biosphere reserve, West Bengal, India. Environ. Dev. Sustain. 23 (8), 1515715182. Springer.
Moniruzzaman, M., Thakur, P.K., Kumar, P., Ashraful Alam, M., Garg, V., Rousta, I., Olafsson, H., 2021. Decadal urban land use/land cover changes and its impact on surface runoff potential for the Dhaka city and surroundings using remote sensing. Rem. Sens. 13 (1), 83.
Morshed, S.R., Fattah, M.A., Haque, M.N., Morshed, S.Y., 2021. Future ecosystem service value modeling with land cover dynamics by using machine learning based Artificial Neural Network model for Jashore city, Bangladesh. Phys. Chem. Earth 103021. Parts A/B/C.
Morshed, S.R., Fattah, M.A., Hoque, M.M., et al., 2022. Simulating Future Intra-urban Land Use Patterns of a Developing City: a Case Study of Jashore, Bangladesh. Geo Journal.
Nautiyal, G., Nautiyal, G., Sharma, A., 2021. Exploring the relationship between spatio-temporal land cover dynamics and surface temperature over dehradun urban dynamics and surface temperature over dehradun urban. J. Indian Soc. Rem. Sens. 49, 1307–1318.
Neill, C.R., Oberhagemann, K., McLean, D., Ferdous, Q.M., 2010. River training works for Padma multipurpose bridge, Bangladesh. In: IABSE-JSCE Joint Conference on Advances in Bridge Engineering-II, pp. 441–448.
Obilor, E.I., Amadi, E.C., 2018. Test for significance of Pearson's correlation coefficient (r). Int. J. Innov. Math. Stat. Energy Pol. 6 (1), 11–23.
Ophra, S.J., Begum, S., Islam, R., et al., 2018. Assessment of bank erosion and channel shifting of Padma River in Bangladesh using RS and GIS techniques. Spat. Inf. Res. 26, 599–605 (2018).
Pal, S., Ziaul, S., 2017. Detection of land use and land cover change and land surface temperature in English Bazar urban centre. Egypt. J. Rem. Sens. Space Sci. 20 (1), 125–145.
RAJUK, 2020. Retrieved from. http://www.rajuk.gov.bd/.
Sedgwick, P., 2014. Spearman's rank correlation coefficient. BMJ 349.
Steeneveld, G.J., Klompmaker, J.O., Groen, R.J.A., Holtslag, A.A.M., 2018. An urban climate assessment and management tool for combined heat and air quality judgements at neighborhood scales. Resour. Conserv. Recycl. 132, 204–217.
Swapan, M.S.H., Zaman, A.U., Ahsan, T., Ahmed, F., 2017. Transforming urban dichotomies and challenges of south Asian megacities: rethinking sustainable growth of Dhaka, Bangladesh. Urban Sci. 1 (4), 31.
Thakur, S., Maity, D., Mondal, I., Basumatary, G., Ghosh, P.B., De, T.K., 2020a. Assessment of changes in land use, land cover, and land surface temperature in the mangrove forest of Sundarbans, northeast coast of India, Environment, Development and Sustainability. Springer 22 (3), 1–29.
Thakur, S., Mondal, I., Bar, S., Nandi, S., Das, P., Ghosh, P.B., De, T.K., 2020b. Shoreline changes and its impact on the mangrove ecosystems of some Islands of Indian Sundarbans, North- East coast of India. J. Clean. Prod. 284, 124764. Elsevier, (2020).
Thakur, S., Mondal, I., Ghosh, P.B., Das, P., De, T.K., 2019. A review of the application of multispectral remote sensing in the study of mangrove ecosystems with special emphasis on image processing techniques. J. Spat. Info. Res. Springer Nature.
Trenberth, K.E., 2011. Changes in precipitation with climate change. Clim. Res. 47 (1e2), 123e138.
Zhang, F., et al., 2016. Dynamics of land surface temperature (LST) in response to land use and land cover (LULC) changes in the Weigan and Kuqa river oasis, Xinjiang, China. Arabian J. Geosci. 9, 1–14, 499.
Zhang, M., Zhang, C., Kafy, A.-A., Tan, S., 2022. Simulating the relationship between land use/cover change and urban thermal environment using machine learning algorithms in Wuhan city, China. Land 11, 14.
Zhang, Y., et al., 2013. NDVI-based vegetation changes and their responses to climate change from 1982 to 2011: a case study in the Koshi River Basin in the middle Himalayas. Global Planet. Change 139–148, 108.
Zhi, Yin, Shan, Liang, Ke, Lina, Yang, Ruxin, 2020. Analysis of land surface temperature driving factors and spatial heterogeneity research based on geographically weighted regression model. Complexity 2020, 2862917.